

# Physical and Statistical Modeling of Saturn's Troposphere

Padmavati A. Yanamandra-Fisher, Amy Braverman, Glenn S. Orton  
Jet Propulsion Laboratory, 4800 Oak Grove Drive, Pasadena, USA

## ABSTRACT

The 5.2- $\mu\text{m}$  atmospheric window on Saturn is dominated by thermal radiation and weak gaseous absorption, with a 20% contribution from sunlight reflected from clouds. The striking variability displayed by Saturn's clouds at 5.2  $\mu\text{m}$ <sup>1</sup> and the detection of PH<sub>3</sub> (an atmospheric tracer) variability near or below the 2-bar level and possibly at lower pressures provide salient constraints on the dynamical organization of Saturn's atmosphere by constraining the strength of vertical motions at two levels across the disk. We analyse the 5.2- $\mu\text{m}$  spectra of Saturn by utilising two independent methods: (a) physical models based on the relevant atmospheric parameters and (b) statistical analysis, based on principal components analysis (PCA), to determine the influence of the variation of phosphine and the opacity of clouds deep within Saturn's atmosphere to understand the dynamics in its atmosphere.

**Keywords:** Saturn, Planetary Atmospheres, Spectroscopy, Phosphine, Statistical Methods, PCA

## 1. INTRODUCTION

Saturn displays striking variability at 5.2  $\mu\text{m}$ <sup>1</sup>. Figure 1 shows 5.2- $\mu\text{m}$  images of Saturn over a five-year interval. A 5.2- $\mu\text{m}$  spectrum of Saturn (from the Infrared Space Observatory, ISO, Short-Wavelength Spectrometer observations<sup>2</sup>) indicating the spectral signatures of several species is shown in Figure 2. This atmospheric window is dominated by thermal radiation and weak gaseous absorption, with a 20% contribution from sunlight reflected from clouds. The radiance variations across Saturn's disk contain a strong axisymmetric component as well as large discrete features at low latitudes. The lack of any morphological correlation between the 5.2- $\mu\text{m}$  features and features at shorter wavelengths that are dominated by reflected sunlight, together with preliminary radiative transfer calculations, indicate that the observed changes result from variations of either the properties of clouds or the mixing ratio of PH<sub>3</sub> near or below the 1-bar level. Does the variability of outgoing radiance arise from variations of cloud opacity or from PH<sub>3</sub> abundance?

PH<sub>3</sub> was suspected as a major influence on Saturn's infrared spectrum<sup>3</sup> and was confirmed by high-resolution spectroscopy<sup>4</sup>. An analysis of Saturn's 5- $\mu\text{m}$  spectrum<sup>5</sup> yielded a PH<sub>3</sub> mixing ratio of  $1 \times 10^{-6}$  for pressures of 400 mbar or less and a mixing ratio of  $7 \times 10^{-6}$  for pressures greater than 400 mbar, using portions of the spectrum dominated by reflected sunlight and by thermal emission, respectively. Analysis of Saturn spectra, obtained by the ISO/SWS, are consistent with a mixing ratio of  $2.5 \times 10^{-6}$  at 300 mbar, assuming (1) a value of  $4.5 \times 10^{-6}$  at the 600-mbar level and deeper in the atmosphere, and (2) a drop off from the 300-mbar level to a value of  $1 \times 10^{-9}$  at 150 mbar<sup>2</sup>. In the submillimeter regime, the analysis of the 1-0 and 3-2 PH<sub>3</sub> transitions in Saturn's disk near 267 and 800 GHz ( $8.9$  and  $26.7 \text{ cm}^{-1}$ )<sup>6,7</sup>, helped derive a global-mean vertical profile for the PH<sub>3</sub> mixing ratio. This profile, showing a constant value for pressures greater than 600 mbar and falling off exponentially with altitude, is consistent with rapid mixing up to the radiative-convective boundary and vertical transport just above this boundary (by upwelling waves, for example) while it undergoes direct photolysis by ultraviolet radiation and scavenging by the H atoms produced by the photolysis.

The detection of PH<sub>3</sub> variations near or below the 2-bar level and possibly at lower pressures will provide salient constraints on the dynamical organization of Saturn's atmosphere by constraining the strength of vertical motions at two levels across the disk. It is also possible that we could confirm a region of uniform mixing at the deepest level sounded, and thereby verify the standard model presented by Refs. 6,7.

---

Further author information: (Send correspondence to P.Y.-F.)  
E-mail: padma@durga.jpl.nasa.gov, Telephone: 1 818 354 2321

## 2. DATA

### 2.1. Data Acquisition

The 5.2- $\mu\text{m}$  spectra of Saturn were acquired 15 - 16 October 2000 at the NASA/InfraRed Telescope Facility (IRTF), Mauna Kea, Hawaii, with a new, moderate-resolution facility near-infrared spectrograph, SpeX. Orton was a co-investigator in both programs. SpeX covers 0.8 to 5.5  $\mu\text{m}$ , providing maximum simultaneous wavelength coverage at a spectral resolving power that is well matched to many planetary features while separating sky emission lines adequately and dispersing the sky continuum. This design requirement has resulted in an instrument which provides spectral resolutions of  $R \sim 1000\text{--}2000$  across two wavelength ranges, 0.8–2.5  $\mu\text{m}$  and 2.0–5.5  $\mu\text{m}$ , using prism cross-dispersers. SpeX also contains an infrared slit-viewer/guider covering a 60 x60 arcsec field of view at 0.12 arcsec/pixel. A Raytheon 1024x1024 InSb array is used in the spectrograph and a Raytheon 512x512 InSb array in the guider<sup>8,9</sup>. The slit was aligned to be parallel to Saturn's rotational axis and perpendicular to the equator. Two types of observations were made. One was straightforward, with the slit fixed on the central meridian for a long integration for high SNR spectra. The disadvantage of this approach was that we were unable to determine whether we were sampling regions of particularly high or low radiance that are prominent in the remarkable 5.2- $\mu\text{m}$  images<sup>1</sup>. We also took a time sequence of spectra with the same slit orientation but were offset from the center of the planet in discrete steps: starting off the east limb of Saturn, taking spectra in 1-arcsec steps westward, and ending off the west limb. Figure 3 shows a sample spectral scan in the 5.2- $\mu\text{m}$  window for Saturn and a calibration star,  $\delta$  Tau. The spectral scan can be projected into an "image cube" of Saturn, two wavelengths of which are shown in Figure 4. The spectral resolution  $R \sim 2000$  and spatial resolution  $\sim 5000$  km on Saturn. The spectra were taken in single-beam mode, with the sky beam simply subtracted from the signal beam. The length of the slit was sufficient to observe the sky off the planet, serving as a check on the background subtraction and the level of observational noise. Observations of the IRTF dome were made for "flat" frames that allow correction of the pixel-to-pixel response variation across the detector. Wavelength calibration is derived from telluric lines in the observations of reference stars ( $\delta$ Tau and  $\iota$ Cap) that also served as standard flux calibrators.

### 2.2. Data Reduction

Data reduction is performed by first extracting spectra from the echelle spectral image that is focused on the SpeX detector using software provided by the IRTF staff<sup>10</sup>. Named Spextool, the code is an interactive IDL-based algorithm that maps the appropriate locus of points in the echelle image onto a spectral continuum which is tagged by wavelength. Each location of the slit that is on the disk of Saturn is time-tagged, and an existing planetary ephemeris program from our IDL-based imaging Data Reduction Manager ("DRM") is used to assign a location on the disk which is verified using the simultaneous measurements of the slit-viewer guider. Together, this information will be used to calibrate the geometry of the spectrum at each observed point on the disk, *i. e.* its latitude, System-III longitude, angle of emission, and angle of incident sunlight. The signal-to-noise ratio (SNR) for the spectral observations of Saturn is high enough to allow the development of models for the distribution of  $\sim 2$ -bar clouds and  $\text{PH}_3$  across the planet. Phosphine is detected in the 4.8- - 5.0- $\mu\text{m}$  interval, with  $\text{NH}_3$  in the 5.1 - 5.3- $\mu\text{m}$  region. Weaker signatures of other species are evident such as  $\text{CH}_3\text{D}$ ,  $\text{AsH}_3$ .

## 3. PHYSICAL MODELS

### 3.1. $\text{PH}_3$ Model

Analysis of the 4.8–5.2  $\mu\text{m}$  region of Saturn's spectrum will be done using a radiative transfer code that accounts for full multiple scattering. We expect that most of the modulation of the radiation, a combination of reflected sunlight and thermal emission, will come from variations of the optical depth of  $\text{NH}_3$  or deeper clouds, but we will determine the variation of  $\text{PH}_3$  abundance near 2 bar from lines near the longer-wavelength thermal emission part of the spectral window, and near 500 mbar from lines near the shorter-wavelength reflected sunlight part of the spectral window. Several bands of  $\text{PH}_3$  appear between 4.3 and 5  $\mu\text{m}$ :  $\nu_1$ ,  $\nu_3$ ,  $2\nu_2$ ,  $2\nu_2$ , and  $\nu_2+\nu_2$ . For completeness, we will include the contributions of gaseous opacities arising from minor and trace constituents, such as  $\text{AsH}_3$ ,  $\text{NH}_3$  and  $\text{CH}_3\text{D}$ . The initial vertical distribution of  $\text{PH}_3$  in Ref. 7 will be perturbed in order to match the radiance at any given location. Molecular spectroscopic parameters are taken from the GEISA data

base<sup>11</sup>, with PH<sub>3</sub> collision-induced line widths taken from Ref. 12. A continuum opacity arising from the collision-induced dipole of H<sub>2</sub>, as influenced by H<sub>2</sub> and He collisions, will be modeled following Birnbaum *et al.* (1996). The mixing ratios of H<sub>2</sub> and He were assumed to be 96% and 4%, respectively (Conrath *et al.* 1984).

### 3.2. Atmospheric Model

The cloud model, adopted from ISO results<sup>2</sup>, consists of two cloud levels: one at 500 mbar pressure with a reflection coefficient of 0.08, and the other at 1.5 bar with a transmission of 0.128. The upper cloud acts primarily to reflect sunlight, and the lower cloud acts to attenuate thermal emission. The optical thickness of these two clouds is varied in order to match “continuum” radiances at the short- and the long-wavelength sides of the spectral window, respectively. We assume the temperature profile and composition (except for PH<sub>3</sub>) given by the ISO SWS spectral analysis<sup>13</sup>. There are not very significant differences between this profile and others, such as those derived from Voyager IRIS observations<sup>14</sup> or the Voyager radio occultation experiment<sup>15</sup> at and below the 1-bar level.

## 4. RADIATIVE TRANSFER ANALYSIS

Our procedure in modeling each spectrum will be first to vary the cloud opacity to match the spectrum in a continuum region near 5.1  $\mu\text{m}$ . Having established the spectral continuum, we will then fit the PH<sub>3</sub> lines by scaling the vertical mixing ratio profile of Ref. 7; We will explore the extent to which we can independently distinguish variations of (a) the PH<sub>3</sub> mixing ratio near and above the 500-mbar level *vs* (b) the opacity of the upper cloud, both of which are constrained by reflected sunlight from the short-wavelength end of the spectrum. Our early results indicate that increasing the abundance of PH<sub>3</sub> increases its absorption and enhances the reflected component of the outgoing radiance; the influence of upper cloud on the outgoing radiance is similar, except no increase in the PH<sub>3</sub> absorption lines is evident; finally, increasing the opacity of the deeper lower cloud affects the 5.1 – 5.3  $\mu\text{m}$  window and the continuum, but not the reflected component of the outgoing radiance.

## 5. STATISTICAL ANALYSIS

### 5.1. Correlation Analysis

A second independent approach to determine the spatial variability of PH<sub>3</sub> and the influence of the deeper clouds in Saturn’s atmosphere on the outgoing radiance in the 5.2- $\mu\text{m}$  window is statistical analysis. Determination of correlations or relationships between various physical parameters can be identified. Correlation coefficients is a simple linear statistical measure between two variables. High or strong correlations result from systematic relations in the atmosphere. The inverse or the existence of high correlation between two parameters indicates that there exists direct or indirect relation between the parameters; with the advantage of the knowledge of one parameter might be a predictor for the second parameter. However, in a system such as Saturn’s atmosphere, with many parameters such as chemical species, clouds and their locations, there are more than just two parameters.

### 5.2. Principal Component Analysis

More advanced statistical approaches such as principal component analysis method (PCA) help in the identification of internal correlations within a data set and allow a linear representation of the statistical data with a minimal number of independent variables. Principal components analysis method identifies the predominant spatial and spectral relationships in the data. PCA has been employed in other branches of sciences such as terrestrial and biology to identify relationships in large data sets. Its application to the fields of planetary and stellar astronomy is more recent, to determine correlations between visible and near-infrared data of various discrete features on Jupiter, from the data returned by *Galileo*<sup>16</sup>; or determining the relationships between optical properties and composition of lunar soil samples<sup>17</sup>. In the field of terrestrial science, PCA is known as Empirical Orthogonal Functions (EOFs) and has been used to denoise data and to capture spatio-temporal relationships<sup>18</sup>.

### 5.3. Spectral Model

The SpeX spectra of Saturn comprise of scans taken parallel to the equator, from the east limb to the west limb, with the 15-arcsec slit of the spectrometer parallel to the rotation axis of the planet. Each scan is a time series of 30 steps or spectral snapshots of a particular latitude band on the planet. To apply PCA method to the data, we divide the 15-arcsec slit into five 3-arcsec intervals to allow the determination of correlations on a finer grid. The wavelengths, for this study, are limited to the 4-8- to 5.2- $\mu\text{m}$  interval, with the user defining the increment or grid in wavelength. The radiance at each of the wavelength on this grid is treated as an independent observation. The data can then be thought of a series of  $30 \times 5$  images, each at one of  $M$  wavelengths. Each of the 150 pixel locations can thus be represented as a point in  $M$ -dimensional space: let  $X_p$ ,  $p = 1, 2, \dots, 150$  be the  $M$ -dimensional column vector of radiances for the  $p$ -th pixel. Principal Component Analysis (PCA) projects the data into a low dimensional subspace of  $\mathcal{R}^M$ ,  $\mathcal{R}^{M'}$   $M' < M$ , such that relationships among data points are preserved as closely as possible. One can then perform exploratory data analysis on the low-dimensional projected data as a proxy for the original.

We standardize each data point using the mean vector and covariance matrix of the entire data set:  $Z_p = \Lambda^{-1/2}(X_p - \bar{X})$ , where  $\bar{X}$  is the column vector of wavelength means, and  $\Lambda$  is an  $M \times M$  matrix containing the wavelength variances on the diagonal and zero elsewhere.  $\Lambda = \text{Diag}(\Sigma)$ .

$$\bar{X} = \frac{1}{150} \sum_{p=1}^{150} X_p, \quad (1)$$

$$\Sigma = \left[ \frac{1}{150} \sum_{p=1}^{150} X_p X_p^t \right] - \bar{X} \bar{X}^t. \quad (2)$$

This transformation compensates for statistical scale differences among wavelengths. The correlation matrix of the original data set is calculated as the covariance matrix of the standardized data:  $\rho = \left[ \frac{1}{150} \sum_{p=1}^{150} Z_p Z_p^t \right]$ . The  $M$  eigenvectors of  $\rho$  form an orthonormal basis in a rotated coordinate system. The eigenvector corresponding to the largest eigenvalue is the direction of maximum variation in the rotated coordinate system. The eigenvector corresponding to the second largest eigenvalue is the direction maximum variation in the remaining  $M - 1$  eigendirections, and so forth. Typically, the first  $M'$  eigenvectors account for most of the variation in the data. This allows us to create an approximation to the standardized version of the original data set using only  $M'$  dimensions:

$$Z'_p = \sum_{m'=1}^{M'} a_{m'p} L_{m'}$$

where  $L_{m'}$  is the  $m'$ -th eigenvector and  $a_{m'p}$  is its weight. If  $M = M'$  then  $Z_p$  is reconstructed exactly. Otherwise,  $Z'_p$  is an approximation.

Our initial focus is the identification of spectral relationships, to determine the spatial variability of  $\text{PH}_3$  in Saturn's atmosphere and compare with the results of radiative transfer analysis. We consider each  $X_p$  as a statistically independent observation representative of conditions in Saturn's atmosphere. We do not distinguish among different regions of the planet or atmosphere. Testing for robustness of the method and validating the results from physical models, we perform the analysis to identify different spatial and temporal relationships.

### ACKNOWLEDGMENTS

This research was performed at the Jet Propulsion Laboratory, California Institute of Technology under contract with NASA.

### REFERENCES

1. Yanamandra-Fisher, P. A., G. S. Orton, B. M. Fisher, and A. Sanchez-Lavega. 2001. Saturn's 5.2- $\mu\text{m}$  cold spots: Unexpected cloud variability. *Icarus* **150**, 189–193.

2. de Graauw, T., H. Feuchtgruber, B. Bézard, P. Drossart, Th. Encrenaz, D. A. Beintema, M. Griffin, A. Heras, M. Kessler, K. Leech, E. Lellouch, P. Morris, P. R. Roelfsema, M. Roos-Serote, A. Salama, B. Vandenbussche, E. A. Valentijn, G. R. Davis, and D. A. Naylor. 1997. First results of ISO-SWS observations of Saturn: Detection of CO<sub>2</sub>, CH<sub>3</sub>H<sub>2</sub>H, C<sub>4</sub>H<sub>2</sub> and tropospheric H<sub>2</sub>O. *Astron. Astrophys.* **321**, L13 - L16.
3. Gillett and Forrest. 1974. The 7.5- to 13.5- $\mu$ m spectrum of Saturn *astrophys. J.* **187**, L37.
4. Bregman, J. D., D. F. Lester, and D. M. Rank. 1975. Observation of the  $\nu_2$  band of PH<sub>3</sub> in the atmosphere of Saturn. *Astrophys. J.* **202** L55-L56.
5. Noll, K. S. and H. P. Larson. 1990. The spectrum of Saturn from 1990 to 2230 cm<sup>-1</sup>: Abundances of AsH<sub>3</sub>, CH<sub>3</sub>D, CO, GeH<sub>4</sub>, NH<sub>3</sub> and PH<sub>3</sub>. *Icarus* **89**, 168 - 189.
6. Orton, G. S., E. Serabyn, and Y. T. Lee. 2000. Vertical distribution of PH<sub>3</sub> in Saturn from observations of the 1-0 and 3-2 rotational lines. *Icarus* **146**, 48-59.
7. Orton, G. S., E. Serabyn, and Y. T. Lee. 2001. Corrigendum: Vertical distribution of PH<sub>3</sub> in Saturn from observations of the 1-0 and 3-2 rotational lines. *Icarus* **149**, 489-490.
8. Rayner, J. T., D. W. Toomey, P. M. Onaka, A. J. Denault, W. E. Stahlberger, D. Y. Watanabe and S. I. Wang. 1998. SpeX: a medium-resolution IR spectrograph for IRTF. *Proc. SPIE* **3354**, 468-479.
9. Rayner, J. T., D. W. Toomey, P. M. Onaka, A. J. Denault, W. E. Stahlberger, W. D. Vacca, and M. C. Cushing. 2002. SpeX: A Medium-Resolution 0.8-5.4 micron Spectrograph and Imager for the NASA Infrared Telescope Facility. (In Preparation).
10. Cushing, M. *et al.* 2002. (In preparation).
11. Jacquinet-Husson, N., E. Arie, A. Barbe, L. R. Brown, B. Bonnet, C. Camy-Peyret, J.-P. Champion, A. Chedin, A. Chursin, C. Clerbaux, G. Duxbury, J.-M. Flaud, N. Fourrie, A. Fayt, G. Graner, R. R. Gamache, A. Goldman, G. Guelachvili, J. M. Hartmann, J. C. Hilco, G. Lefevre, V. Naumenko, A. Nikitin, A. Perrin, D. Reuter, L. Rosenmann, L. S. Rothman, N. A. Scott, J. Selby, L. N. Sinita, J. M. Sirota, A. Smith, K. Smith., V. G. Tyuterevi, R. H. Tipping, S. Urban, P. Varanasi, and M. Weber. 1999. The 1997 spectroscopic GEISA databank. *J. Quant. Spectrosc. Rad. Transfer.* **62**, 205-254.
12. Lévy, A., N. Lacombe, and G. Tarrago. 1993. Hydrogen- and helium-broadening of phosphine lines. *J. Mol. Spectrosc.* **157**, 172-181.
13. Bézard, B. 2000. Spectroscopy of Solar System Objects. *ESA-SP 456*.
14. Conrath, B. J. and J. A. Pirraglia. 1983. Thermal structure of Saturn from Voyager infrared measurements - Implications for atmospheric dynamics. *Icarus* **53**, 286-292.
15. Lindal, G. F., J. R. Lyons, D. N. Swetnam, V. R. Eshleman, D. P. Hinson. 1987. The atmosphere of Uranus - Results of radio occultation measurements with Voyager 2. *JGR* **92**, 14987-15001.
16. Dyudina, U. A., A. P. Ingersoll, G. E. Danielson, K. H. Baines, R. W. Carlson and The Galileo NIMS Team. 2001. Interpretation of NIMS and SSI Images on the Jovian Cloud Structure. *Icarus*, **150**, 219 - 233.
17. Pieters, C. M., D. G. Stankevich, Yu. G. Shkuratov and L. A. Taylor. 2002. Statistical Analysis of the Links among Lunar Mare Soil Mineralogy, Chemistry, and Reflectance Spectra. *Icarus*, **155**, 285 - 298.
18. Preisendorfer, R. W. *Principal Component Analysis in Meteorology and Oceanography*, Elsevier, New York, 1988.

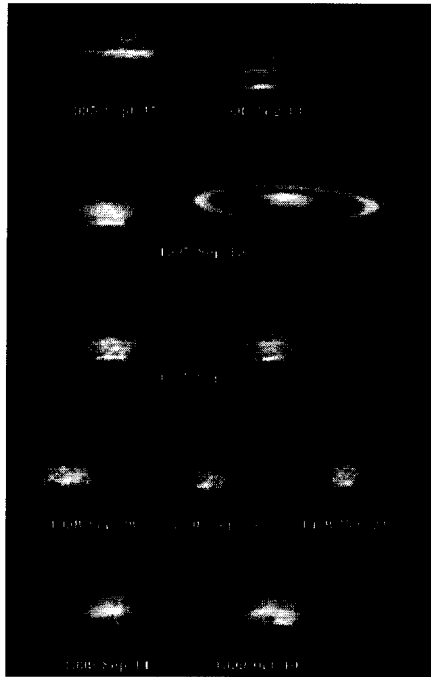


**Figure 1.** Images of Saturn at  $5.2 \mu\text{m}$  from IRTF observing runs between 1995 and 1999. At this wavelength, the outgoing radiation is dominated by thermal emission. The image from 1995 September 17 was made using a filter centered at  $4.8 \mu\text{m}$  whose spectral function is shown in Figure 2 and which is affected by a greater contribution of sunlight reflected from Saturn's upper clouds. Note that the ring obscuration is apparent as a dark band in the upper half of the images, except for the 1995 image which was taken when the rings were nearly edge on. A comparison image taken with a broad filter centered at  $0.86 \mu\text{m}$  using a camera at the Pic du Midi one rotation earlier on 1998 November 23 is also shown for comparison. The visible feature just south of the equator corresponds to an area just to the left of a subtle dark spot at the same latitude in the adjacent  $5.2\text{-}\mu\text{m}$  image. There is no apparent correlation between discrete features in either image.

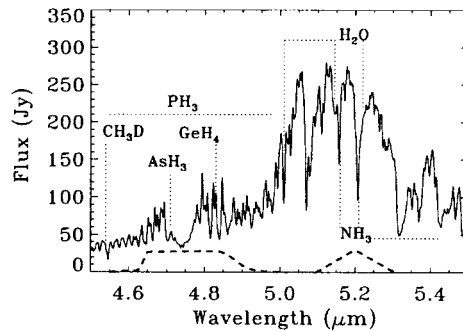


**Figure 2.** Saturn's spectrum from the ISO Short-Wavelength Spectrometer (SWS), taken from Ref. 2. The spectral filter functions for the NSFCAM  $5.2\text{-}\mu\text{m}$  circular variable filter position and for the discrete filter centered at  $4.8 \mu\text{m}$  (the 1995 data shown in Figure 1) are also shown.

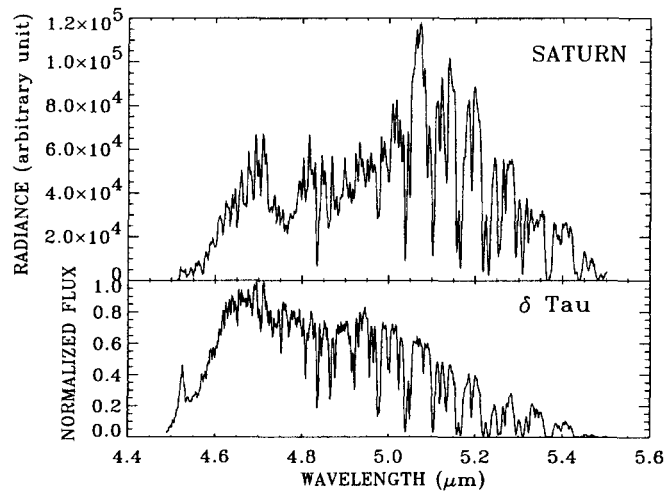


**Figure 3.** Sample SpeX spectra of Saturn, corresponding to one scan from the east limb to the west limb, taken at NASA/IRTF, with a slit of 0.8" X 15", oriented parallel to the rotation axis of Saturn, LCM<sub>III</sub> of 140° W. A sample spectrum of the calibration star,  $\delta$  Tau, is also illustrated. The spectra exhibit high S/N.

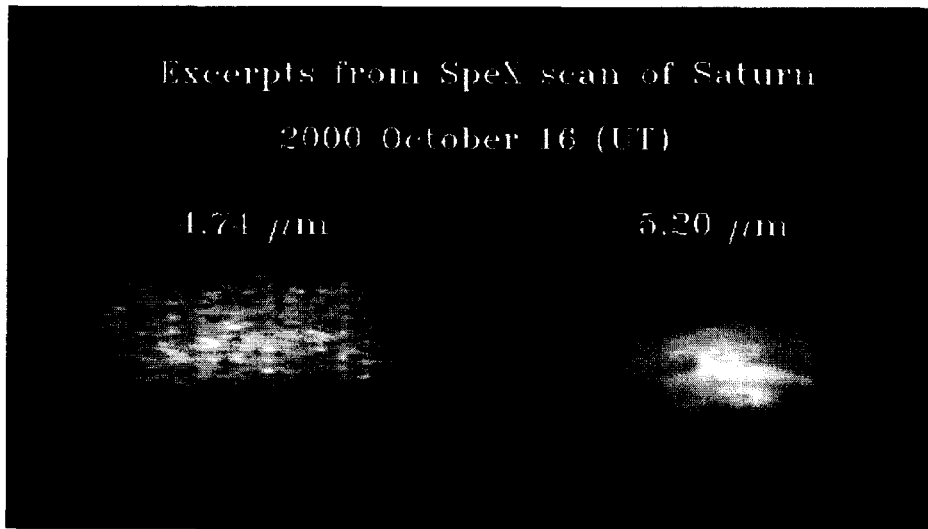


**Figure 4.** “Images” of Saturn at two wavelengths, corresponding to the low and upper end of the 5- $\mu$ m window, created from the SpeX spectral scan illustrated in Figure 3. The lower end near 4.7  $\mu$ m is sensitive to the reflected component of Saturn radiance and exhibits no distinct features; the image at 5.2  $\mu$ m probes around 2 – 2.5 bar and displays cold spots, warm regions and marked banded structure, indicative that the opacity of the lower deeper cloud influences the variability observed.